Earth and Planetary Science Letters 454 (2016) 78–85

Contents lists available at ScienceDirect

Earth and Planetary Science Letters

www.elsevier.com/locate/epsl

Extensional extrusion: Insights into south-eastward expansion of Tibetan Plateau from magnetotelluric array data

Hao Dong [a,b,*], Wenbo Wei [a,b], Sheng Jin [a,b], Gaofeng Ye [a,b], Letian Zhang [a,b], Jian'en Jing [a,b], Yaotian Yin [a,b], Chengliang Xie [a,b], Alan G. Jones [c,d,a]

[a] School of Geophysics and Information Technology, China University of Geosciences, Beijing, China
[b] State Key Laboratory of Geological Processes and Mineral Resources, China University of Geosciences, Beijing, China
[c] Dublin Institute for Advanced Studies, Dublin, Ireland
[d] Complete MT Solutions, Ottawa, Canada

ARTICLE INFO

Article history:
Received 30 March 2016
Received in revised form 20 July 2016
Accepted 25 July 2016
Available online xxxx
Editor: P. Shearer

Keywords:
magnetotellurics
resistivity structure
Tibetan Plateau
eastward expansion
extensional extrusion
SINOPROBE

ABSTRACT

Despite extensive effort over many decades to understand the tectonic evolution of the Tibetan Plateau, the geodynamic processes creating the iconic south-eastward expansion of the plateau at the Eastern Himalayan Syntaxis (EHS) are still unclear and are hotly debated. Two popular (but not necessarily exclusive) geodynamic models, namely crustal flow at mid-to-lower crustal depths and coherent deformation between the crust and lithospheric mantle, are commonly invoked to explain the expansion mechanism. However, neither of these is able to reconcile all of the abundant geological and geophysical data. Here we present a three-dimensional (3D) geo-electrical model, derived from new SINOPROBE magnetotelluric (MT) array data, that reveals the geo-electrical, and by inference rheological, structure of southeast Tibet. Instead of NW–SE conductive channels proposed in prior two-dimensional (2D) MT studies, distinct NNE–SSW directed quasi-linear conductive anomalies are identified in the mid-to-lower crust, which are separated by a large-scale electrically resistive structure that extends from the crust to the upper mantle. This argues against the prior proposed model of south-eastward conductive anomalies, and hence against the southeast lower crust flow of material. To interpret our observations and resultant model, a new mechanism of "extensional extrusion" is proposed to address the lithospheric deformation of the south-eastward expansion of Tibetan Plateau.

1. Introduction

The continuous collision and convergence procedure between Indian and Asian plates has generated the Tibetan Plateau and the immense east–west mountain range of Himalaya since ~55 Ma (Royden et al., 2008; Tapponnier, 2001). This nearly 3000 km orogenic belt terminates at both ends in almost transverse syntaxes, namely the Western Himalayan Syntaxis and Eastern Himalayan Syntaxis (EHS, Fig. 1). At the east end, the strong crustal deformation has resulted in the uplift and southeast-ward expansion of East Tibet by ~8 to 10 Ma (Royden et al., 2008; Tapponnier, 2001). Geodetic studies also reveal fast on-going southeast-ward surface movement near the EHS (Zhang et al., 2004). However, the mechanisms for the plateau deformation and expansion remain subjects of debate. There are two canonical theses of (i) rigid block extrusion (Tapponnier et al., 1982) and (ii) internal deformation (England and Houseman, 1986) for the expansion mechanism. (i) suggests the landmass of Tibet fails (in a brittle manner) into several rigid blocks bounded by strike-slip faults as India collides into Asia. These blocks then extrude along these strike-slip faults to southeast into Indochina as the collision continues. On the other hand, (ii) assumes a more ductile Asia and suggests the deformation and expansion is internally continuous in the crust and upper mantle over broad areas (Klemperer, 2006).

Recent geophysical and geoid evidence tends to favour more than one type of internal deformation. Some involve crustal flow in restricted zones/layers (Clark et al., 2005) and others involve vertically coherent deformation (Bendick and Flesch, 2007; Sol et al., 2007). The major conflict between these two internal deformation paradigms lies in the degree of mechanical (de)coupling of the crust and the lithospheric mantle. For example, south-eastward lower crustal flow decoupled from the upper crust and mantle is supported by localised reduced resistivity (Bai et al., 2010) and

* Corresponding author at: School of Geophysics and Information Technology, China University of Geosciences, Beijing, China.
E-mail address: donghao@cugb.edu.cn (H. Dong).

http://dx.doi.org/10.1016/j.epsl.2016.07.043
0012-821X/

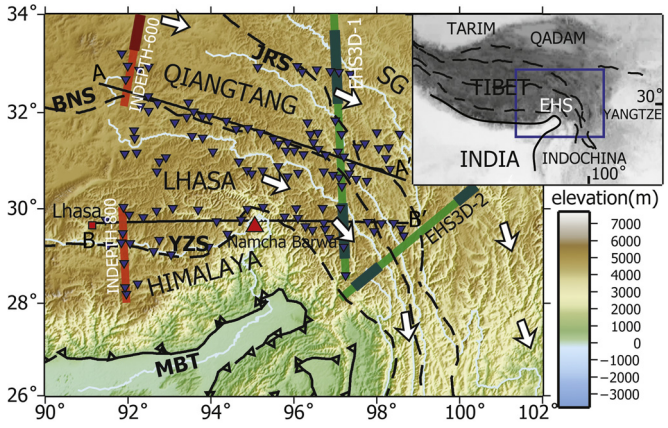

Fig. 1. Topographic map of southeast Tibet Plateau superposed with major thrusts and suture zones. The magnetotelluric stations used in the inversion and interpretation are shown in blue triangles. Previously proposed crustal flow channels are shown as white arrows (Bai et al., 2010). The green and orange lines show the previous profiles of project EHS3D and INDEPTH respectively. The darker portion in the profiles indicates the location with enhanced conductivity presented in previous publications (Bai et al., 2010; Unsworth et al., 2005). EHS: Eastern Himalayan Syntaxis; YZS: Yarlung-Zampo Suture; BNS: Bankong-Nujiang Suture; JRS: Jinsha River Suture; MBT: Main Boundary Thrust; SG: Songpan-Ganzi Terrance. (For interpretation of the references to colour in this figure legend, the reader is referred to the web version of this article.)

Vs velocity (Liu et al., 2014). However, continuous crustal flow over long distances seems unlikely with the strong NW–SE lateral heterogeneity revealed by ambient noise interferometry (Yang et al., 2012) and receiver function studies (Wang et al., 2010). Conversely, vertically coherent deformation is supported by consistent GPS surface motion and mantle seismic anisotropy (Sol et al., 2007; Wang et al., 2008). Strong coupling between the lithospheric mantle and the crust is challenged by the contrasting anisotropies of the lower crust and upper mantle revealed by a Rayleigh wave dispersion study (Yao et al., 2010). All of these contradictions suggest that the geodynamic processes responsible for the expansion are far more complex than we have predicted in the past and may not be explained by a single simple mechanism. Hence, robust and higher resolution constraints on the physics and rheology of the crust and upper mantle are crucially needed to understand the true expansion process(es) of Southeast Tibet.

2. Magnetotelluric data and analysis

The magnetotelluric (MT) method measures natural time-varying electromagnetic waves on the surface to probe the subsurface electrical conductivity (σ, the inverse of resistivity $\rho = 1/\sigma$) (Chave and Jones, 2012). Since MT is sensitive to interconnected conductive hydrous fluids and melt phases, it has been widely used to constrain the presence of fluids and the rheology of the crust and mantle (Le Pape et al., 2015). As a part of the China-wide, multi-discipline geophysical deep probing project SINOPROBE (Dong et al., 2013), data from 290 MT stations were acquired in the study region from 2010 to 2012. The magnetotelluric stations of the SINOPROBE project were recorded using commercial MT instruments, namely Phoenix MTU-5 (broadband MT) and LVIV LEMI-417 (long period MT) systems. Electric and magnetic field time series were measured parallel and perpendicular to geomagnetic north. Typical recording time of the station was 24 h for broadband MT and 7 d for long period MT. The time series were processed using a statistically robust algorithm (Egbert and Booker, 1986) with remote reference technique (Gamble et al., 1979) to calculate MT transfer functions. The transfer functions were obtained with a broad period range of ~0.01 to ~6000 s, which is more than sufficient for probing into the upper mantle despite the relatively low resistivity in the lower crust. The transfer functions were rotated to geographical north according to the local magnetic declination. Thanks to the very low local population density and cultural noise level, the data are generally of good to excellent quality.

The new dataset fills the extensive gaps between the former 2D MT observation profiles (Bai et al., 2010; Li et al., 2003; Wei et al., 2001) and extends them to a 3D array covering the EHS and the southeast margin of Tibetan Plateau (Fig. 1). For the first time, we provide insight into the 3D geo-electrical structure of the region. The extreme regional topography was a severe challenge for data acquisition and explains the uneven site distribution (Fig. 1). A few sites that are strongly distorted by the extreme topography are not used for the inversion. Since inversion schemes may tend to over-fit the densely covered areas and left the other areas under-fitted, the data were selected for inversion to achieve as uniform a site distribution (Dong et al., 2014) as possible in order to avoid biased fitting induced by locally differential station distribution.

In 2D interpretations of MT, we make an approximation that magnetotelluric data can be separated into two independent modes, namely transverse electric (TE) mode and transverse magnetic (TM) mode, which corresponds to electric current flow along and across strike respectively (Chave and Jones, 2012). As the approximation may no longer be valid in a 3D earth, applying 2D methods to a 3D dataset can lead to misinterpretation of the underground structure (Garcia et al., 1999; Ledo, 2005). Phase tensor analysis (Caldwell et al., 2004) is hence derived to test the dimensionality of the resistivity of crust and upper mantle. As the depth of penetration of MT signal differ with period and the conductivity structure, the phase tensor data are plotted at a constant penetration depth rather than a constant period. The estimation of penetration depth uses the Niblett–Bostick transformation method (Jones, 1983). A Berdichevsky average for XY and YX mode of apparent resistivity is used for the Niblett–Bostick transformation to convert periods (frequencies) to depths. The data are hence selected at the corresponding periods to calculate the phase tensors. The orientations of the phase tensor ellipses indicate the direction of preferred current flow and reflect lateral conductivity variations of the underground structures, while circular ellipses show little or no major lateral variations (one dimensional structure) (Caldwell et al., 2004; Hill et al., 2009). The colours filling the phase tensor ellipses show the phase tensor skew angle β and indicate the asymmetry in the MT response, which reflects 3D structures. Please note that $\Phi(2 \times \beta)$ is plotted here instead of β to better displaying the asymmetry of the MT responses (Booker, 2013).

At 5 km, the orientations of phase tensor ellipses show a generally NNE–SSW direction in the northern part of the study region (Fig. 2a). The generally light colours of the PT skew angles suggest a 1D or quasi-2D structure in the uppermost crust. As depth increases the orientation of the phase tensor ellipses rotates to a dominant NWW direction across the whole study area (Figs. 2b–d). Regional geo-electrical structures can thus be inferred to be differently directed in the upper crust and in the lower crust/upper mantle. The extremely flattened ellipses in the lower crust suggest the existence of abrupt lateral geo-electrical interfaces parallel or perpendicular to the surface tectonics. The overall dark colours of the PT skew angles ($>5°$) reflect highly asymmetric conductive structures, which indicates regional 3D structures.

3. Magnetotelluric inversion

One hundred and seventeen out of the total 290 stations were inverted with a 3D modular electromagnetic inversion code (ModEM) utilizing nonlinear conjugate gradient optimising method

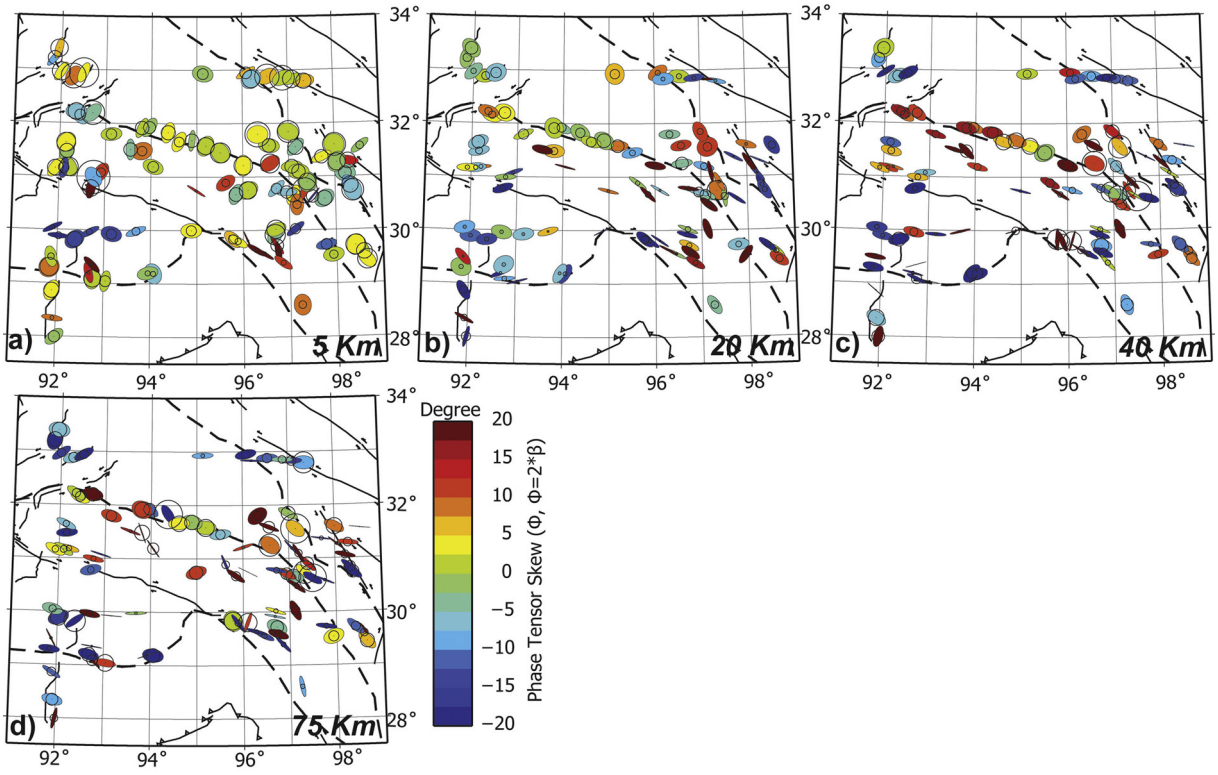

Fig. 2. Maps of magnetotelluric phase tensors ellipses. Because signal penetration depends on period, ellipses at the same approximate depth of penetration (5 to 75 km) are plotted (see text for discussion). Please note that only the stations used in the inversion and interpretation are plotted.

(Egbert and Kelbert, 2012). The initial inversion model was constructed with a horizontally uniform 8 by 8 km mesh within the array area and a progressingly increasing mesh with a ratio of 1.5 outside the area. The vertical mesh started with a relatively shallow layer of 30 m, allowing the inversion scheme to generate minor (shallow) structures to address any local galvanic distortion/topographic effects (Dong et al., 2014). The starting model is set to homogeneous 100 Ωm (0–670 km) with a 3 Ωm basement (>670 km) to ensure the lower boundary condition of the transition zone in mantle (Booker et al., 2004). MT transfer functions at 24 periods from 0.01 to 6000 s were used in the inversion, with an error floor set to 5% of the $|Zxy * Zyx|^{0.5}$ for the full impedance tensor (diagonal and off-diagonal elements). The preferred model is obtained after 217 iterations, with a normalized misfit of 2.05 (from a starting model misfit of 11.27). The model responses are generally well fit with the observed data (Figs. S1–S4, Supplementary Material). Horizontal slices of the preferred model at different depths are shown in Fig. 3.

Below the relatively resistive upper crust (Fig. 3a) our model reveals widespread conductors (∼2–20 Ωm) in the mid-to-lower crust of the study region (Figs. 3b–c). Isolated conductors first emerge at the bottom of upper crust (15–20 km, Fig. 3b). They start to interconnect with each other and form N–S or NNE–SSW directed structures in the lower crust to upper mantle (Figs. 3c–d). Perhaps the most intriguing, surprising and unexpected feature of the model is a moderately resistive to resistive (∼300–3000 Ωm) structure (labelled R1) that extends from the upper mantle to the crust and from the Jinsha River Suture (JRS) to the Yarlung-Zangpo Suture (YZS) near Namcha Barwar (Fig. 1). Perpendicular to the surface structures, the NNE–SSW striking R1 truncates the relatively conductive mid-to-lower crust and upper mantle into two separated regions labelled C1 and C2 (Figs. 3c–d). The abrupt changes of resistivity are also consistent with the geo-electric interfaces indicated by phase tensor analysis.

As ModEM utilizes a structured 3D cuboid mesh (Kelbert et al., 2014), the model regularization scheme would tend to generate smooth structures along the mesh grids (x, y, or z axes). Hence the interconnection of N–S/NNE–SSW structures of our model may be a product of grid orientation. To test this possibility, we ran the inversion procedure with data rotated by 45° clockwise, which is equivalent to rotating the grid 45° counter clockwise. The same major anomalies can still be found in the test model, suggesting that the N–S/NNE–SSW directed structures are robust (Fig. S5, Supplementary Material). The minor differences between the rotated and original models probably came from the data variance difference from the rotation procedure of magnetotelluric transfer functions.

A previous 2D MT study with separated profiles (Bai et al., 2010) interpreted the locations of increased conductivity (dark colour in the profiles EHS3D-1 and EHS3D-2, Fig. 1) as two NW–SE directed lower crustal conductive channels. It is believed that the enhanced conductivity is induced by fluids, which lower the viscosity of the lower crust and permit south-eastward lower crust (pipe) flows that decouples from upper mantle and upper crust (Bai et al., 2010). While a certain degree of congruity can be found between the prior 2D model and our corresponding 3D cross-section (Fig. 4), the conductive structures strike distinctly NNE–SSW in our 3D map (Figs. 3c and 3d) instead of NW–SE as inferred in the 2D study. Apparently, NNE directed crustal flows would drive the Tibetan Plateau north-eastward instead of south-eastward, which are not reconcilable with the observed surface motions. This demonstrates the well-known poor off-profile constraint (Kiyan et al., 2014) when performing 2D MT modelling of 3D data, especially when the vertical field transfer functions, which are highly sensitive to off-profile structures, are not included in the interpretations.

It is nevertheless tempting to attribute the conductive anomalies to the existence of south-eastward lower crustal flow if the separated C1 and C2 conductors can be connected to each other

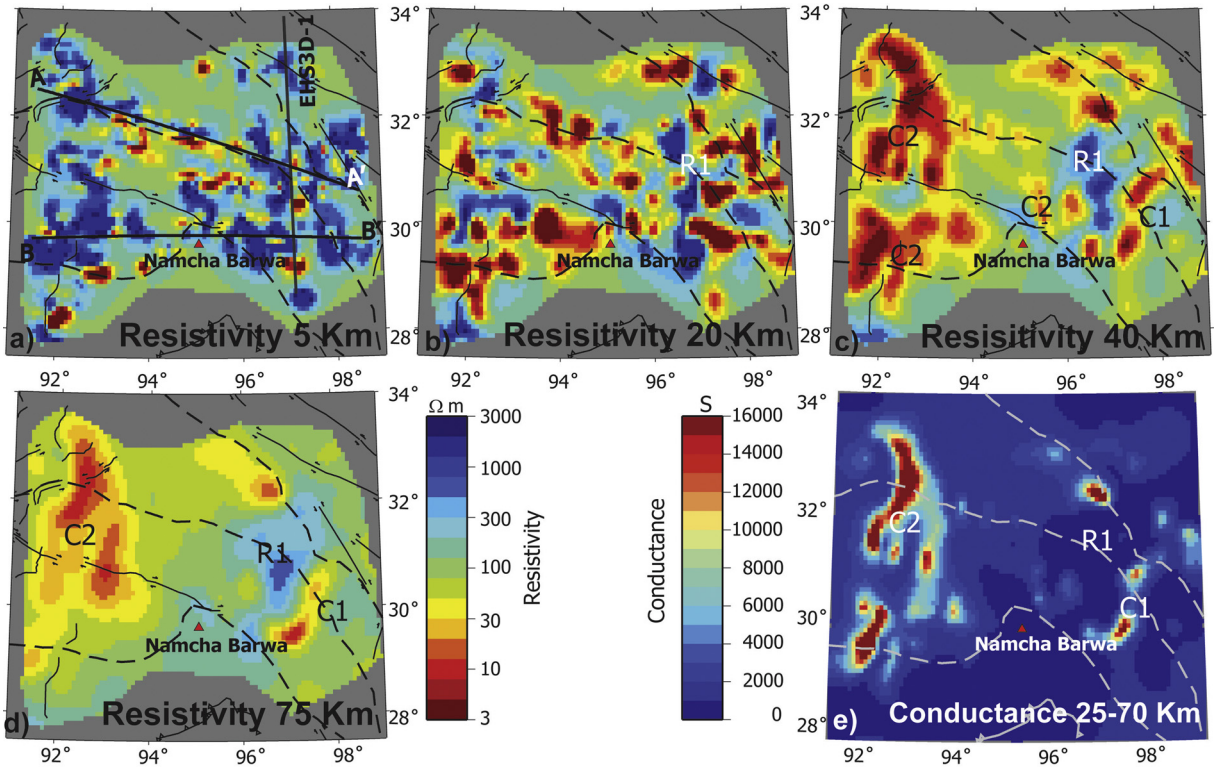

Fig. 3. Resistivity maps at depths from 5–75 km (a–d) and depth-integrated conductance map calculated for mid-to-lower crust (25–70 km) (e). (For interpretation of the references to colour in this figure legend, the reader is referred to the web version of this article.)

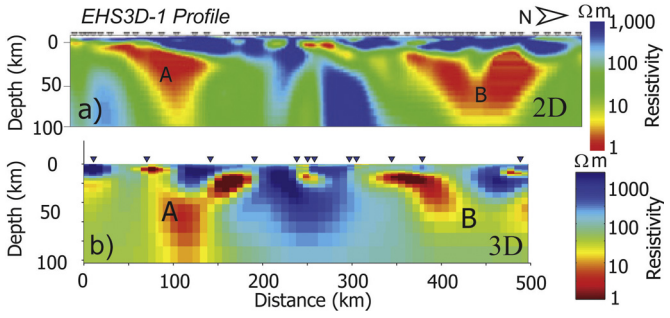

Fig. 4. Comparison of the geo-electric resistivity sections between a) profile EHS3D-1 from a previous 2D MT study (Bai et al., 2010) and b) the corresponding cross section from 3D MT interpretation. Note the two sub-figures use different colour scales.

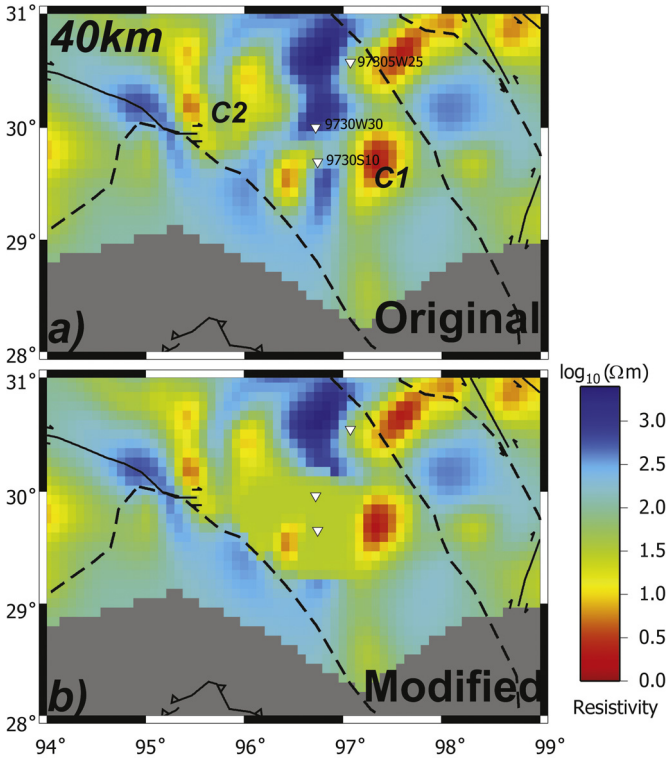

Fig. 5. Resistivity maps of the feature test models at 40 km. a) Original preferred model of 3D magnetotelluric inversion. b) Modified model with a conductive channel connecting C1 and C2.

in some manner. To test this possibility, a moderate conductive (30 Ωm) channel connecting C1 and C2 in the mid-to-lower crust (Fig. 5) is introduced to the preferred model. A second inversion is performed using the modified model as the starting model, but with the conductive channel fixed (i.e. not allowed to change in the inversion). However, the data cannot be fit in the inversion with this channel. Although the overall misfit of the second inversion is just slightly larger than the original inversion (2.10 vs 2.05), it should be noted that responses from the second inversion seem to be much rougher than the original response, especially for the impedance phases (Fig. 6). This indicates that the second inversion cannot find any model that fit the data with the same smoothing factor of the original inversion. Hence the inversion scheme has to reduce the smoothing factor and generate more structures ("rougher") than the original model. Still, the regional apparent resistivity responses in the period range of 10–3000 s are strongly changed (by 0.5–1 log magnitude, Fig. 6), which are larger than the data uncertainties (10% in apparent resistivity). Therefore a connection between C1 and C2 is rejected by the data. Interestingly, apart from the stations right above the channel, a few stations far from the introduced conductive feature are still able to sense the change of resistivity (Fig. 6c). This may indicate the introduced

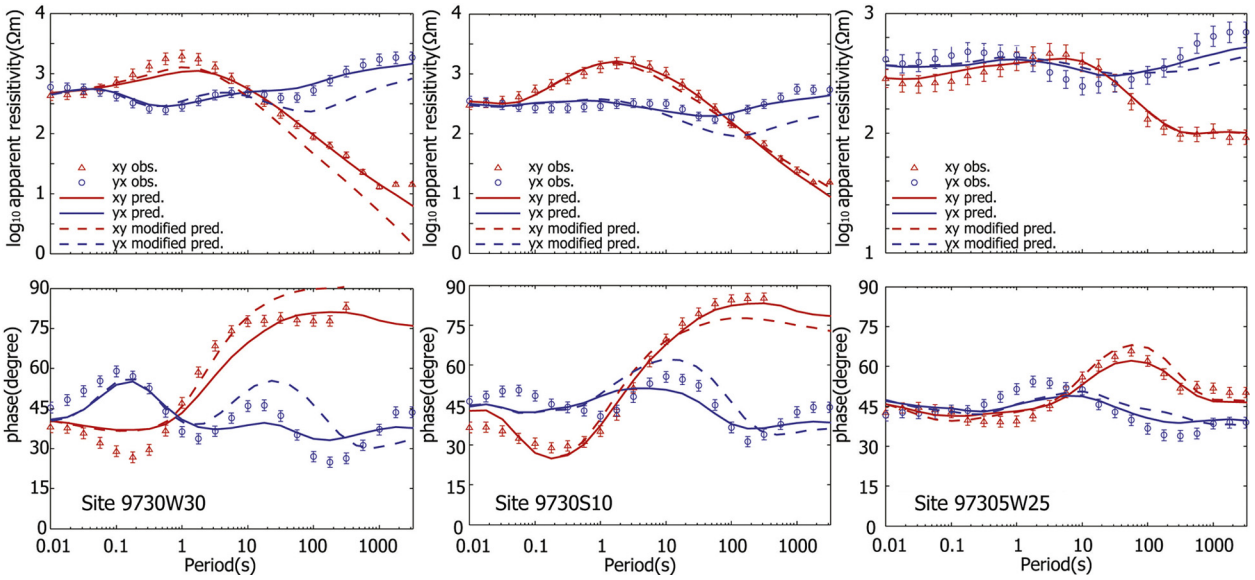

Fig. 6. MT observed and predicted data from station 9730W30, 9730S10 and 97305W25 in the model feature test. The triangles and circles show the observed data. The error bars for the observed data are the modified error floors used in the inversion and exceed or equal to observed error bars. The dashed lines indicate the response of the model feature test, whereas the solid lines show the response of original model. The locations of the stations are shown in Fig. 5.

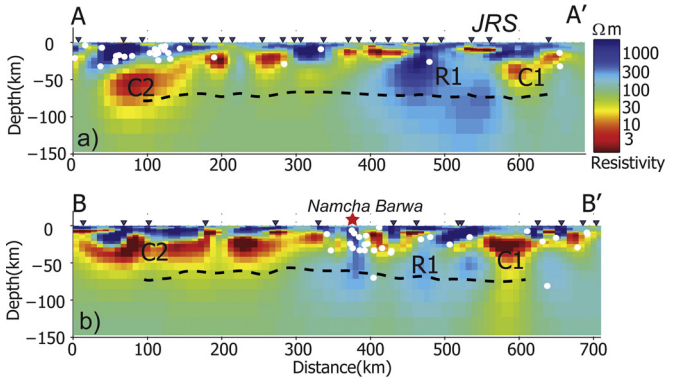

Fig. 7. Resistivity sections under profiles A–A', B–B' shown in Fig. S3. The white dots show the seismicity ($M_w > 4.0$) within a range of 15 km from the profiles between 2000 and 2015 (seismicity data downloaded from http://www.csndmc.ac.cn). See captions in Fig. 1 for profile locations and aberrations. The dash lines indicate the Mohorovičić discontinuity estimated by seismic receiver function (Xu et al., 2013).

conductive channel has a more than local effect on electric current flow pattern.

4. Discussion

Broadly coincident with mapped high heat flow (Hu et al., 2000) and low Vs (Ceylan et al., 2012) zones, the predominant mid-to-lower crust conductive anomalies can be attributed to partial melts, with co-existing hydrous fluids, as suggested in previous studies (Li et al., 2003; Rippe and Unsworth, 2010; Unsworth et al., 2005). Hydrous fluids will begin to induce partial melt at temperature ~620 °C (Thompson and Connolly, 1995). Given the high heat flow (~80 mW/m^2) in the study region, the temperature can be reached at ~22 km (Hu et al., 2000). Hence conductive anomaly caused solely by aqueous fluid is not possible below 22 km. The general absence of seismicity within these conductive structures (Fig. 7) also suggests that the conductors are too weak/ductile to produce earthquakes, which supports the argument for the presence of fluid. The few seismic events at the conductive boundaries may be triggered by fluid infiltration from the conductors (Wannamaker et al., 2009). Hence the question arises as to whether these partial melts/hydrous fluids facilitate south-eastward crustal flow, or whether these fluids induce the decoupling of the crust and upper mantle?

4.1. Estimation of fluids content

Conductance can be used to estimate the fluid fraction and the viscosity of the crust (Le Pape et al., 2015). MT data generally provide a better resolved estimate of the conductance of a particular layer (i.e. the depth-integrated conductivity) rather than its actual resistivity (Jones, 1992). The depth-integrated conductance can be estimated by calculating the $S = h/\rho$ of each layer over the given depth range. The fluid fraction can be estimated as two-phase media using Archie's law:

$$\sigma_{\text{eff}} = C\Phi^n\sigma_f \tag{1}$$

where σ_{eff} is the effective conductivity, Φ is the fluid fraction, σ_f is the conductivity of the fluid, with $C = 1.64$ and $n = 1.34$ be Archie's empirical coefficients (ten Grotenhuis et al., 2005).

If the MT method detects a conductor, there is ambiguous interpretation of its cause, such as fluids, metasediments, iron oxides, etc. Conversely, when MT sees a resistive region, any interconnected conducting mechanism, including those mentioned above, can be excluded. Fig. 3e shows the integrated conductance calculated using the preferred resistivity model from 25 to 70 km. Between the bright C1 and C2 conductors, the conductance in R1 is generally <1000 S (Fig. 3e, dark blue). Previous geophysical studies suggest a flow channel thickness of ~20–30 km (Bai et al., 2010; Liu et al., 2014). However, only a minor fluid fraction of 0.52% to 2.15% with a fluid resistivity of 0.05 Ωm to 0.2 Ωm (5–20 S/m) is needed for the observed conductance (Bai et al., 2010) in such a layer. This will produce a relatively high effective viscosity comparable with typical stable continental lower crust (~10^{21}–10^{23} Pa/s) (Rippe and Unsworth, 2010), which correlates well with the high seismic Q value revealed by Lg-wave Q tomography (Zhao et al., 2013).

By contrast, the conductance of N–S/NNE–SSW striking C1 and C2 is mostly greater than 8000–10000 S (Fig. 3e, yellow to red colour). To achieve such conductance in a 20–30 km thick conductive layer, a far higher fluid fraction (3.7% to 12.6%) is needed for a fluid phase with the same resistivity as before. This may imply much lower viscosity in the lower crust in C1 and C2 than in R1.

4.2. Possibility of crustal flows

Two major physical simplifications, Poiseuille flow and Couette flow, are commonly used to address the lower crustal flow patterns. Poiseuille flow involves flow between stationary boundaries while Couette flow involves shear flow between moving boundaries. Previous studies assume a hybrid Couette/Poiseuille flow driven by pressure gradients from topographic (downslope) variation in the study region (Klemperer, 2006; Rippe and Unsworth, 2010). Assuming Airy type isostatic compensation, the pressure gradient can be calculated with Kruze et al. (1991):

$$\nabla p \approx \left(\frac{\rho_m - \rho_c}{\rho_m}\right)\frac{\rho_c g \Delta h}{L/2} \tag{2}$$

where ∇p is the pressure gradient, Δh is the topographic variation over a distance L, ρ_c and ρ_m are crust and mantle densities. Assuming a crust density of 2600 kg/m^3 and a mantle density of 3300 kg/m^3, the lateral pressure gradient can be calculated with the topographic variation Δh and distance L of the flow. For the region around the EHS, the Δh is $<$1000 m in a relative long distance L of about 600 km from $\sim$92°E to $\sim$98°E. The pressure gradient generated is therefore much smaller ($<$18 Pa/m) than the gradient of the north margin of Tibetan Plateau (120 Pa/m) (Le Pape et al., 2015) or the central part of Tibetan plateau (80 Pa/m) (Rippe and Unsworth, 2010). As the viscosity will be lowest at the channel boundaries where the shear stress is highest, the minimum effective viscosity is given by Turcotte and Schubert (1982):

$$\eta_{\text{eff}} = -\frac{h^2}{8(n+2)\bar{u}}\frac{dp}{dx} \tag{3}$$

where $\bar{u}$ is the average velocity of the flow, h is the thickness of the flow layer, $n = 1.8$ is the power law for non-Newtonian fluid. For a non-Newtonian fluid, the effective viscosity will vary with strain rate. For partially molten granites, the strain rate of the flow can be estimated using the empirical equation (Rutter et al., 2006):

$$\frac{d\epsilon}{dt} = A\exp(B\Phi^m)\exp(-H/RT)\sigma^n \tag{4}$$

where $d\epsilon/dt$ is strain rate, σ is flow stress, T is temperature, Φ is melt fraction, R is the gas constant, with the fitted parameters $\log(A) = -1.39$, $n = 1.8$, $m = 2$, $B = 192$ and $H = 220 \pm 65$ KJ/m (Le Pape et al., 2015). The effective viscosity can be calculated using the following approximation (Godin et al., 2006):

$$\eta_{\text{eff}} \approx \sigma/(d\epsilon/dt) \tag{5}$$

Therefore the fluid fraction of a certain crust composition can also be estimated as a function of effective viscosity, temperature and strain rate.

Now given a flow layer of 20–30 km, to create an observed surface speed of 0.5–1 cm/yr in the region (Gan et al., 2007), apparently the speed of the hybrid flow should be higher than a pure Couette type (0.25–0.5 cm/yr, half of the surface speed). A relatively low viscosity ($\sim$1.5–6.7 $\times$ 10^{18} Pa s) is needed for the flow speed. The regional crustal strain rate is in the range of 7–10 nstrain/yr basing on previous GPS crust motion measurements (Gan et al., 2007). At the temperature of lower crust (800–1000 °C), the viscosity requires far higher fluid/melts fraction in the lower crust ($\sim$12–18%) than we have estimated in R1 ($<$2.15%). Therefore lower crust flow in electrically and mechanically resistive R1 can be excluded.

4.3. The extensional extrusion process

Based on the strong rheological heterogeneity in the study region, we propose an "extensional extrusion" model for the geodynamic process of southeast Tibet Plateau. In this scenario, the lithosphere around the Eastern Himalayan Syntaxis experiences major N–S/NNE–SSW directed compressive stress and perpendicular extensional stress (Jiménez-Munt and Platt, 2006). Therefore the extensional stress introduces localised extension of lithosphere and creates weakened passages for hydrous fluids/partial melts (Fig. 8a). Induced by the subducting Indian plate, hot upwelling material starts to rise from the upper mantle through these weak areas and introduces fluids to the mid-to-lower crust. The upwelling and lateral spreading of the fluids lowers the viscosity locally and gradually pushes the crust away from these weak zones. The crust then appears to "spread" sideways with E–W/NW–SE extension, just like the seafloor spreading process at mid-ocean ridges (Fig. 8b). The accumulation of these local extensions results in the onset of the near E–W extension of Tibetan Plateau in Cenozoic (Royden et al., 2008). Blocked by the stable Yangtze Craton to the east, the landmass is then pushed and extruded south-eastward by the E–W extension (Clark and Royden, 2000). This produces a tangential clockwise surface velocity field around the EHS (Fig. 8b, blue arrows). Combining the tangential velocity with the radial velocity from the India–Asia collision (Fig. 8b, red arrows), the total velocity field is directed from NE to E, which

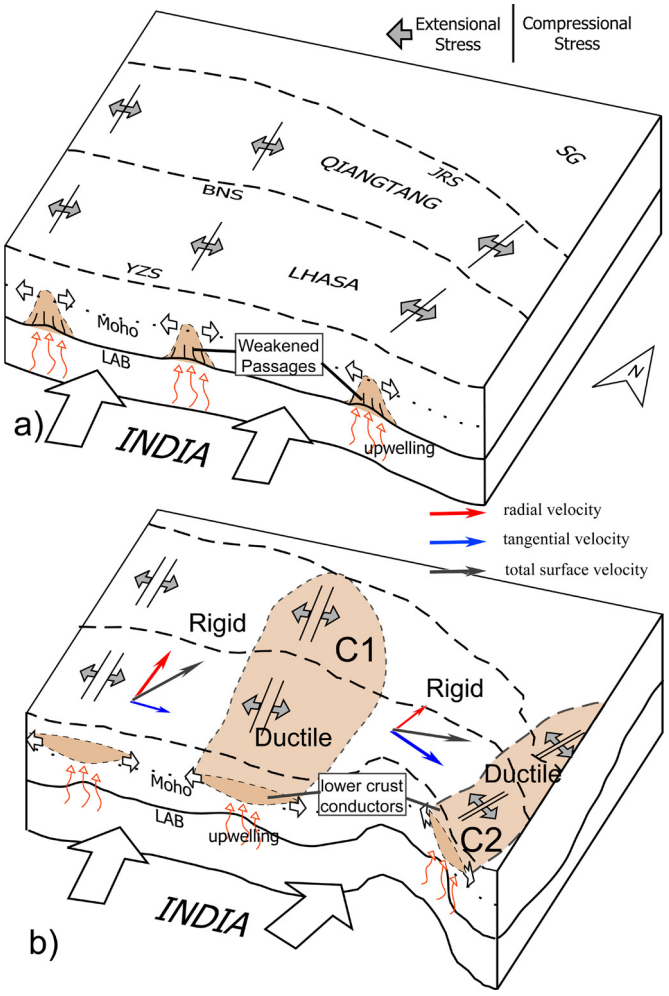

Fig. 8. Schematic illustration of the extensional extrusion process of southeast Tibet. a) The upwelling of fluids/partial melts and the initial stage of the E–W extensions. b) The lateral spreading of the fluids and the further extrusion caused by extension processes. The shaded regions indicate the accumulated fluid/melts in the lower crust. The open arrows show the movement of tectonic units, while the closed arrows show predicted surface motion. See Fig. 1 for tectonic abbreviations. (For interpretation of the references to colour in this figure legend, the reader is referred to the web version of this article.)

is consistent with surface GPS velocity measurements (Gan et al., 2007). On the other hand, parts of the lower crust not affected by these fluids/partial melts may well remain at relatively higher viscosity (rigid). This strong rheological contrast therefore contributes to the complex 3D geo-electrical and velocity responses in the region (Yang et al., 2012; Yao et al., 2010).

Unlike the rigid block extrusion model, which assumes brittle failure and strike-slip extrusion of the Tibetan landmass, our model suggests that the extrusion of the plateau material may be caused by the accumulated "spreading" of a series of locally ductile E–W extension zones. Similarly, our model could explain the (slower) north-westward surface motion near Western Himalayan Syntaxis at the west end of Tibetan Plateau (Zhang et al., 2004). However, like any solid material, crust cannot extend without limit, especially for the less ductile upper crust. Eventually the ductile extensions lead to brittle failure of upper crust, which might be the cause of the north–south directed extensional rift systems in central Tibetan Plateau.

5. Conclusions

In this study, high-quality magnetotelluric array data covering Eastern Himalayan Syntaxis are analysed and modelled. For the first time a 3D resistivity model of southeast Tibetan Plateau around the EHS is presented, revealing strong lateral variations in electrical resistivity in the mid-to-lower crust. Prominent NNE–SSW directed conductive anomalies are revealed to be separated by large scale resistive structure in the lower crust. The resistivity variations are attributed to strong lateral rheological heterogeneity, which is not consistent with the previously proposed mechanism of "south-eastward crustal flow" for the eastward expansion of Tibetan Plateau. To interpret the geo-electrical variation and to explain the geodynamic process near the EHS, we present a new "Extensional Extrusion" model. The south-eastward expansion/extrusion of Tibetan Plateau may result from the accumulated east–west spreading of a series of local ductile extensions zones. These extensions accumulated around EHS could also explain the present day clockwise surface motion observed in the region.

Due to the data coverage, our model cannot constrain structures east of 99°E. A carefully designed 3D MT array can test our hypothesis to the east of our study region.

Acknowledgements

This study is supported by project SINOPROBE on sub-project SINOPROBE 01-02 and 01-01. Special thanks must go to our field crews and students; this study would not have been possible without their efforts. The authors thank Chris Beaumont, John Booker, Kate Selway and an anonymous referee for their constructive comments, which greatly improve the manuscript.

Appendix A. Supplementary material

Supplementary material related to this article can be found online at http://dx.doi.org/10.1016/j.epsl.2016.07.043.

References

Bai, D., Unsworth, M.J., Meju, M.a., Ma, X., Teng, J., Kong, X., Sun, Y., Sun, J., Wang, L., Jiang, C., Zhao, C., Xiao, P., Liu, M., 2010. Crustal deformation of the eastern Tibetan Plateau revealed by magnetotelluric imaging. Nat. Geosci. 3, 358–362. http://dx.doi.org/10.1038/ngeo830.

Bendick, R., Flesch, L., 2007. Reconciling lithospheric deformation and lower crustal flow beneath central Tibet. Geology 35, 895. http://dx.doi.org/10.1130/G23714A.1.

Booker, J., Favetto, A., Pomposiello, M., 2004. Low electrical resistivity associated with plunging of the Nazca flat slab beneath Argentina. Nature 429, 399–403. http://dx.doi.org/10.1038/nature02573.1.

Booker, J.R., 2013. The magnetotelluric phase tensor: a critical review. Surv. Geophys. 35, 7–40. http://dx.doi.org/10.1007/s10712-013-9234-2.

Caldwell, T.G., Bibby, H.M., Brown, C., 2004. The magnetotelluric phase tensor. Geophys. J. Int. 158, 457–469. http://dx.doi.org/10.1111/j.1365-246X.2004.02281.x.

Ceylan, S., Ni, J., Chen, J.Y., Zhang, Q., Tilmann, F., Sandvol, E., 2012. Fragmented Indian plate and vertically coherent deformation beneath eastern Tibet. J. Geophys. Res. 117, B11303. http://dx.doi.org/10.1029/2012JB009210.

Chave, A., Jones, A., 2012. The Magnetotelluric Method: Theory and Practice. Cambridge University Press, Cambridge, England.

Clark, M., Royden, L., 2000. Topographic ooze: building the eastern margin of Tibet by lower crustal flow. Geology, 703–706.

Clark, M.K., Bush, J.W.M., Royden, L.H., 2005. Dynamic topography produced by lower crustal flow against rheological strength heterogeneities bordering the Tibetan Plateau. Geophys. J. Int. 162, 575–590. http://dx.doi.org/10.1111/j.1365-246X.2005.02580.x.

Dong, H., Wei, W., Ye, G., Jin, S., Jones, A.G., Jing, J., Zhang, L., Xie, C., Zhang, F., Wang, H., 2014. Three-dimensional electrical structure of the crust and upper mantle in Ordos Block and adjacent area: evidence of regional lithospheric modification. Geochem. Geophys. Geosyst. 15, 2414–2425. http://dx.doi.org/10.1002/2014GC005270.

Dong, S.-W., Li, T.-D., Lü, Q.-T., Gao, R., Yang, J.-S., Chen, X.-H., Wei, W.-B., Zhou, Q., 2013. Progress in deep lithospheric exploration of the continental China: a review of the SinoProbe. Tectonophysics 606, 1–13. http://dx.doi.org/10.1016/j.tecto.2013.05.038.

Egbert, G.D., Booker, J.R., 1986. Robust estimation of geomagnetic transfer functions. Geophys. J. Int. 87, 173–194.

Egbert, G.D., Kelbert, A., 2012. Computational recipes for electromagnetic inverse problems. Geophys. J. Int. 189, 251–267. http://dx.doi.org/10.1111/j.1365-246X.2011.05347.x.

England, P., Houseman, G., 1986. Finite strain calculations of continental deformation: 2. Comparison with the India–Asia Collision Zone. J. Geophys. Res., Solid Earth 91, 3664–3676. http://dx.doi.org/10.1029/JB091iB03p03664.

Gamble, T., Goubau, W., Clarke, J., 1979. Error analysis for remote reference magnetotellurics. Geophysics 44, 959–968.

Gan, W., Zhang, P., Shen, Z.-K., Niu, Z., Wang, M., Wan, Y., Zhou, D., Cheng, J., 2007. Present-day crustal motion within the Tibetan Plateau inferred from GPS measurements. J. Geophys. Res. 112, B08416. http://dx.doi.org/10.1029/2005JB004120.

Garcia, X., Ledo, J., Queralt, P., 1999. 2D inversion of 3D magnetotelluric data: the Kayabe dataset. Earth Planets Space 51, 1135–1143.

Godin, L., Grujic, D., Law, R.D., Searle, M.P., 2006. Channel flow, ductile extrusion and exhumation in continental collision zones: an introduction. Geol. Soc. (Lond.) Spec. Publ. 268, 1–23. http://dx.doi.org/10.1144/GSL.SP.2006.268.01.01.

Hill, G.J., Caldwell, T.G., Heise, W., Chertkoff, D.G., Bibby, H.M., Burgess, M.K., Cull, J.P., Cas, R.a.F., 2009. Distribution of melt beneath Mount St Helens and Mount Adams inferred from magnetotelluric data. Nat. Geosci. 2, 785–789. http://dx.doi.org/10.1038/ngeo661.

Hu, S., He, L., Wang, J., 2000. Heat flow in the continental area of China: a new data set. Earth Planet. Sci. Lett. 179, 407–419.

Jiménez-Munt, I., Platt, J.P., 2006. Influence of mantle dynamics on the topographic evolution of the Tibetan Plateau: results from numerical modeling. Tectonics 25, 1–17. http://dx.doi.org/10.1029/2006TC001963.

Jones, A.G., 1983. On the equivalence of the "Niblett" and "Bostick" transformations in the magnetotelluric method. J. Geophys. 53, 72–73.

Jones, A.G., 1992. Electrical properties of the continental lower crust. In: Fountain, D.M., Arculus, R.J., Kay, R.W. (Eds.), Continental Lower Crust. Elsevier, Amsterdam, pp. 81–143.

Kelbert, A., Meqbel, N., Egbert, G.D., Tandon, K., 2014. ModEM: a modular system for inversion of electromagnetic geophysical data. Comput. Geosci. 66, 40–53. http://dx.doi.org/10.1016/j.cageo.2014.01.010.

Kiyan, D., Jones, A.G., Vozar, J., 2014. The inability of magnetotelluric off-diagonal impedance tensor elements to sense oblique conductors in three-dimensional inversion. Geophys. J. Int. 196, 1351–1364. http://dx.doi.org/10.1093/gji/ggt470.

Klemperer, S.L., 2006. Crustal flow in Tibet: geophysical evidence for the physical state of Tibetan lithosphere, and inferred patterns of active flow. In: Law, R.D., Searle, M.P., Godin, L. (Eds.), Channel Flow, Ductile Extrusion and Exhumation in Continental Collision Zones. Geological Society, London, pp. 39–70. http://dx.doi.org/10.1144/GSL.SP.2006.268.01.03.

Kruze, S., McNutt, M., Phipps-Morgan, J., Royden, L., 1991. Lithospheric extension near lake mead, Nevada: a model for ductile flow in the lower crust. J. Geophys. Res. 96, 4435–4456. http://dx.doi.org/10.1029/90JB02621.

Le Pape, F., Jones, A.G., Unsworth, M.J., Vozar, J., Wei, W., Jin, S., Ye, G., Jing, J., Dong, H., Zhang, L., Xie, C., 2015. Constraints on the evolution of crustal flow beneath Northern Tibet. Geochem. Geophys. Geosyst. 16, 4237–4260. http://dx.doi.org/10.1002/2015GC005828.

Ledo, J., 2005. 2-D versus 3-D magnetotelluric data interpretation. Surv. Geophys. 26, 511–543. http://dx.doi.org/10.1007/s10712-005-1757-8.

Li, S., Unsworth, M., Booker, J.R., 2003. Partial melt or aqueous fluid in the mid-crust of Southern Tibet? Constraints from INDEPTH magnetotelluric data. Geophys. J. Int. 153, 289–304.

Liu, Q.Y., van der Hilst, R.D., Li, Y., Yao, H.J., Chen, J.H., Guo, B., Qi, S.H., Wang, J., Huang, H., Li, S.C., 2014. Eastward expansion of the Tibetan Plateau by crustal flow and strain partitioning across faults. Nat. Geosci. 7, 361–365. http://dx.doi.org/10.1038/ngeo2130.

Rippe, D., Unsworth, M., 2010. Quantifying crustal flow in Tibet with magnetotelluric data. Phys. Earth Planet. Inter. 179, 107–121. http://dx.doi.org/10.1016/j.pepi.2010.01.009.

Royden, L.H., Burchfiel, B.C., van der Hilst, R.D., 2008. The geological evolution of the Tibetan Plateau. Science 321, 1054–1058. http://dx.doi.org/10.1126/science.1155371.

Rutter, E.H., Brodie, K.H., Irving, D.H., 2006. Flow of synthetic, wet, partially molten "granite" under undrained conditions: an experimental study. J. Geophys. Res., Solid Earth 111, 1–17. http://dx.doi.org/10.1029/2005JB004257.

Sol, S., Meltzer, A., Bürgmann, R., van der Hilst, R.D., King, R., Chen, Z., Koons, P.O., Lev, E., Liu, Y.P., Zeitler, P.K., Zhang, X., Zhang, J., Zurek, B., 2007. Geodynamics of the southeastern Tibetan Plateau from seismic anisotropy and geodesy. Geology 35, 563. http://dx.doi.org/10.1130/G23408A.1.

Tapponnier, P., 2001. Oblique stepwise rise and growth of the Tibet Plateau. Science 80 (294), 1671–1677. http://dx.doi.org/10.1126/science.105978.

Tapponnier, P., Peltzer, G., Le Dain, A.Y., Armijo, R., Cobbold, P.R., 1982. Propagation extrusion tectonics in Asia: new insights from experiments with plasticine. Geology 10, 611–616. http://dx.doi.org/10.1130/0091-7613(1982)10<611:PETIAN>2.0.CO;2.

ten Grotenhuis, S.M., Drury, M.R., Spiers, C.J., Peach, C.J., 2005. Melt distribution in olivine rocks based on electrical conductivity measurements. J. Geophys. Res., Solid Earth 110, 1–11. http://dx.doi.org/10.1029/2004JB003462.

Thompson, A.B., Connolly, J.A.D., 1995. Melting of the continental crust: some thermal and petrological constraints on anatexis in continental collision zones and other tectonic settings. J. Geophys. Res. 100, 15,565–15,579. http://dx.doi.org/10.1029/95JB00191.

Turcotte, D.L., Schubert, G., 1982. Geodynamics: Applications of Continuum Physics to Geological Problems, 1st ed. Wiley, New York.

Unsworth, M.J., Jones, A.G., Wei, W., Marquis, G., Gokarn, S.G., Spratt, J.E., Bedrosian, P., Booker, J., Leshou, C., Clarke, G., Shenghui, L., Chanhong, L., Ming, D., Sheng, J., Solon, K., Handong, T., Ledo, J., Roberts, B., 2005. Crustal rheology of the Himalaya and Southern Tibet inferred from magnetotelluric data. Nature 438, 78–81. http://dx.doi.org/10.1038/nature04154.

Wang, C.-Y., Flesch, L.M., Silver, P.G., Chang, L.-J., Chan, W.W., 2008. Evidence for mechanically coupled lithosphere in central Asia and resulting implications. Geology 36, 363. http://dx.doi.org/10.1130/G24450A.1.

Wang, C.-Y., Lou, H., Silver, P.G., Zhu, L., Chang, L., 2010. Crustal structure variation along 30°N in the eastern Tibetan Plateau and its tectonic implications. Earth Planet. Sci. Lett. 289, 367–376. http://dx.doi.org/10.1016/j.epsl.2009.11.026.

Wannamaker, P.E., Caldwell, T.G., Jiracek, G.R., Maris, V., Hill, G.J., Ogawa, Y., Bibby, H.M., Bennie, S.L., Heise, W., 2009. Fluid and deformation regime of an advancing subduction system at Marlborough, New Zealand. Nature 460, 733–736. http://dx.doi.org/10.1038/nature08204.

Wei, W., Unsworth, M., Jones, A., Booker, J., Tan, H., Nelson, D., Chen, L., Li, S., Solon, K., Bedrosian, P., Jin, S., Deng, M., 2001. Detection of widespread fluids in the Tibetan crust by magnetotelluric studies. Science 80 (292), 1999–2001.

Xu, Q., Zhao, J., Pei, S., Liu, H., 2013. Imaging lithospheric structure of the eastern Himalayan syntaxis: new insights from receiver function analysis. J. Geophys. Res., Solid Earth 118, 2323–2332. http://dx.doi.org/10.1002/jgrb.50162.

Yang, Y., Ritzwoller, M.H., Zheng, Y., Shen, W., Levshin, A.L., Xie, Z., 2012. A synoptic view of the distribution and connectivity of the mid-crustal low velocity zone beneath Tibet. J. Geophys. Res. 117, B04303. http://dx.doi.org/10.1029/2011JB008810.

Yao, H., van der Hilst, R.D., Montagner, J.-P., 2010. Heterogeneity and anisotropy of the lithosphere of SE Tibet from surface wave array tomography. J. Geophys. Res. 115, B12307. http://dx.doi.org/10.1029/2009JB007142.

Zhang, P.-Z., Shen, Z., Wang, M., Gan, W., Bürgmann, R., Molnar, P., Wang, Q., Niu, Z., Sun, J., Wu, J., Hanrong, S., Xinzhao, Y., 2004. Continuous deformation of the Tibetan Plateau from global positioning system data. Geology 32, 809. http://dx.doi.org/10.1130/G20554.1.

Zhao, L.F., Xie, X.B., He, J.K., Tian, X., Yao, Z.X., 2013. Crustal flow pattern beneath the Tibetan Plateau constrained by regional Lg-wave Q tomography. Earth Planet. Sci. Lett. 383, 113–122. http://dx.doi.org/10.1016/j.epsl.2013.09.038.